Sensing and Bio-Sensing Research 38 (2022) 100536

Contents lists available at ScienceDirect

Sensing and Bio-Sensing Research

journal homepage: www.elsevier.com/locate/sbsr

A pin-based pyro-electrohydrodynamic jet sensor for tuning the accumulation of biomolecules down to sub-picogram level detection

Simona Itri [a,b], Danila del Giudice [a,b,c], Martina Mugnano [a], Volodymyr Tkachenko [a], Sanna Uusitalo [d], Annukka Kokkonen [e], Inka Päkkilä [e], Heidi Ottevaere [f], Yunfeng Nie [f], Emanuela Mazzon [g], Agnese Gugliandolo [g], Pietro Ferraro [a], Simonetta Grilli [a,*]

[a] Institute of Applied Sciences and Intelligent Systems (ISASI), National Research Council of Italy (CNR), Pozzuoli, NA 80078, Italy
[b] Department of Mathematics, Physics University of Campania, Caserta 81100, Italy
[c] Department of Chemicals, Materials and Production Engineering, University of Naples Federico II, Piazzale Tecchio 80, 80125 Naples, Italy
[d] VTT Technical Research Centre of Finland, Optical Measurements, Kaitoväylä 1, 90570 Oulu, Finland
[e] VTT Technical Research Centre of Finland, Biosensors, Kaitoväylä 1, 90570 Oulu, Finland
[f] Vrije Universiteit Brussel and Flanders Make, Brussel Photonics, Dept. of Applied Physics and Photonics, Pleinlaan 2, 1050 Brussels, Belgium
[g] IRCCS Centro Neurolesi "Bonino-Pulejo", Via Provinciale Palermo, Contrada Casazza, 98124 Messina, Italy

ARTICLE INFO

Keywords:
Alzheimer's disease
Aβ1-42
Biosensors
P-jet

ABSTRACT

The detection of low abundant biomarkers is of great interest in different clinical cases, such as the early diagnosis of Alzheimer's disease. Here we present what we call pin-based pyro-electrohydrodynamic jet (p-jet) sensor that can linearly tune the accumulation rate of biomolecules in tiny droplets. In this newly revealed pin-based configuration we demonstrate the ability to detect biomolecules down to sub-picogram concentration. Two different fluorescent probes at a varying number of accumulated droplets, up to 50, have been used to investigate the p-jet sensor. Moreover, a comparative study with a commercial piezo-driven bio-spotter has been performed. The spots of biomolecules exhibit high reproducibility by achieving a coefficient of variation <10%, both in diameter and fluorescence intensity, respectively. Remarkably, the spot intensity increases linearly with the number of accumulated droplets, thus showing the effective inherent additive functionality of this technique. Such accumulation effect allowed us to reach a limit of detection down to sub-picogram level. The p-jet sensor was applied to detect the Aβ1–42 protein, a typical Alzheimer's disease biomarker, through an immunoreaction protocol carried out on the p-jet spots. The results demonstrate the compatibility of the p-jet with immunoassay procedures, opening the route to the development of a highly sensitive device able to detect low abundant biomarkers for early diagnosis applications.

1. Introduction

Biosensors are devices that usually estimate the level of a biological marker, a so-called biomarker, by producing a measurable signal that is related to the concentration of the analyte involved in the chemical reaction [1]. Biosensors are used in many fields such as the screening of very small molecule libraries as well as in pathologies that require a rapid detection of biomarkers and continuous monitoring [2], for instance in the detection of harmful bacteria [3,4]. Biosensors can be divided in different categories according to their principles of operation such as enzyme-based [5,6], optical [7,8], and aptamer-based [9], just to name a few. Even though their performance is sufficient for a wide range of applications, existing biosensors are struggling, when the abundant biomarker concentration in biological samples is very low (< 10 pg/mL). In such cases, the limit of detection (LOD) of the standardized techniques often prevents clinicians and/or biologists from using biosensors to perform their studies. One of the open issues is the current lack of a reliable technique for quantifying the levels of Alzheimer's disease (AD) biomarkers in the peripheral blood of clinical patients [10]. Nowadays this analysis can only be performed from cerebrospinal fluid (CSF) samples, which entail sufficient biomarker dosage. CSF sampling has a dramatic impact on the patient in terms of invasiveness and on the health service in terms of hospitalization required for performing such tests. Moreover, the invasiveness of the procedure prevents the

* Corresponding author.
E-mail address: simonetta.grilli@isasi.cnr.it (S. Grilli).

https://doi.org/10.1016/j.sbsr.2022.100536
Received 8 June 2022; Received in revised form 29 September 2022; Accepted 13 October 2022
Available online 14 October 2022

clinicians to perform screening tests among the populations and follow-up therapies on full-blown patients. The gold standard for quantifying the levels of AD biomarkers in CSF is represented by ELISA-based procedures, which reach a LOD of around 50 pg/mL. Conversely, the level in the peripheral blood is expected to be <1 pg/mL. It has been shown that an innovative label-free electrochemical protein sensor by Mundelanji Vestergaard et al. and a new colorimetric sensor by Ajay Piriya V·S. et al. could reach the LOD above 10 pg/mL [11,12]. This is an improvement to the current level of ELISA tests, but there is still a need for one-decade improvement in sensitivity to reach the required level for peripheral blood. Different innovative techniques have been proposed in literature to overcome the limit. These include mass spectrometry [13,14], immunoprecipitation [15] and SIMOA [16]. These methods have a high precision to identify and quantify the biomarker concentrations, but they include laborious and crucial pre-treatments of the sample [17] that may reduce the level of reproducibility. Moreover, the complexity and costs of these procedures prevent their use in routine clinical assays.

Recently we proposed the pyroelectric effect as an innovative and successful tool for microprinting of different fluids and polymers for soft matter manipulation application [18,19], or for fabricated scaffolds for cells [20,21] or even for dispensing biomolecules [22]– [24]. Moreover, we used this effect for accumulating low abundant biomolecules, thus significantly increasing the signal-to-noise ratio in fluorescence-based assays. We demonstrated this useful capability in case of oligonucleotides, gliadin [24], lactose [22] and collagen [23], by using pre-labelled molecules. The related results showed clearly how the technique, that we call 'pyro-electrohydrodynamic jet' (p-jet), has the potential for opening the route to a completely new technology for high-sensitive biosensors. Although the proof of concept behind the p-jet sensor appears mature, still some work was needed to fill the gap toward the real-world usage in biomedicine and for implementing a benchtop reliable biosensor.

Here, we present a significant step forward in the development of this technology by implementing a new configuration of the p-jet, which allows us to tune the accumulation rate of the low abundant biomolecules. In this work we show that a reliable and reproducible configuration can be realized thus overcoming the previous critical limitations. The new key innovation relies on loading the sample solution in a commercial microarray-printing pin, which allows us to produce a stable meniscus profile from which the tiny droplets are ejected with high reproducibility. We used specific fluorescent probes[24] for demonstrating the reproducibility of the spots and successfully attaining a linear trend of the fluorescent signal as a function of the number of accumulated jets, down to sub-picogram level. Moreover, a comparative study is also accomplished and discussed with respect to a commercial piezo-driven bio-spotter, demonstrating the ability of p-jet to accumulate low abundant biomolecules and to make them detectable down to sub-picogram concentrations. Finally, we applied the technique to the case study of the Alzheimer's disease by detecting low abundant Aβ1–42 biomarker in spots obtained through the p-jet accumulation effect and subjected successively to an immunoassay reaction. The achieved results demonstrate for the first time the possibility to use the p-jet accumulation in immunoassay protocols, with the key advantage to use a volume of reaction below the microliter range, thus pushing the limit of detection beyond what is typically encountered in commercial ELISA kits (Invitrogen, Cat. KHB3441). We believe that this technique would open the route to the development of a highly sensitive device able to detect low abundant biomarkers for early diagnosis applications.

2. Materials and methods

2.1. Lithium niobate and the pyroelectric effect

Lithium niobate (LN) is a rhombohedral crystal belonging to the point group 3 m. The crystals were bought from Crystal Technology Inc. in the form of both sides polished 500 μm thick c-cut 3-in. wafers. The wafers were cut into 2 cm^2 sized samples by a standard diamond saw. The spontaneous polarization P_s changes according to the following: $\Delta P_i \propto p_i \Delta T$. P_i is the coefficient of the polarization vector, p_i is the pyroelectric coefficient and ΔT indicates the variation of temperature. At equilibrium, without thermal stimulation, the spontaneous polarization is compensated by the external screening charge and no electric field is present. When the crystal is subject to a temperature variation, a surface charge density $\alpha = p_i \Delta T$ appears locally due to uncompensated charges. Consequently, a high electric field ($\sim 10^7$ V/m) is generated on the surface of the crystal.

2.2. Target slide

In case of the fluorescent probes, we used a standard 1 mm thick microscope glass slides, without specific surface functionalization. Conversely, in case of the immunoassay application, we used glass slides functionalized with 2D-Amine groups (PolyAn GmbH, Germany) and with a standard size of 25 × 75 × 1 mm. In this case, the surface is functionalized by NH_3^+ groups for non-covalent coupling of negatively charged biochemical species via electrostatic adsorption.

2.3. Printing pin

The pin is a commercial microarray stealth printing pin (SMP3, Arrayit Corporation) usually employed for contact printing of microarray slides [25]. Fig. 1(a,b) show two optical microscope images of the pin at different magnifications, while Fig. 1(c) shows a sketch of the pin tip, with the characteristic dimensions. Here, we load the sample in a sample well and we use for the first time an electric field for drawing tiny droplets from the pin, avoiding contact on the slide.

2.4. Fluorescent probes

We used two kinds of fluorescent probes: the Alexa Fluor 647 fluorophore, a far-red-fluorescent dye (cat. no. A33084, life technologies), and a secondary antibody conjugated with a fluorophore, the Alexa Fluor Plus 647 (cat. no. A32733, life technologies). The fluorophore was bought as powder and dissolved in 1× Phosphate Buffered Saline (Life technologies Cat.N. 10,010,023), at a concentration of 1.25 mg/mL, the solution was mixed gently to ensure the solubilization of the powder. Starting from this solution, 20 μL, 9.6 μL and 5 μL were diluted in 2 mL of PBS (Phosphate-buffered saline) 1×, each one, to have the final concentrations of 12.5 μg/mL, 6 μg/mL and 3 μg/mL. The secondary antibody was bought as a solution with initial concentration of 1 mg/mL and diluted in dH_2O at the final concentrations of 10 pg/mL, 0.1 pg/mL and

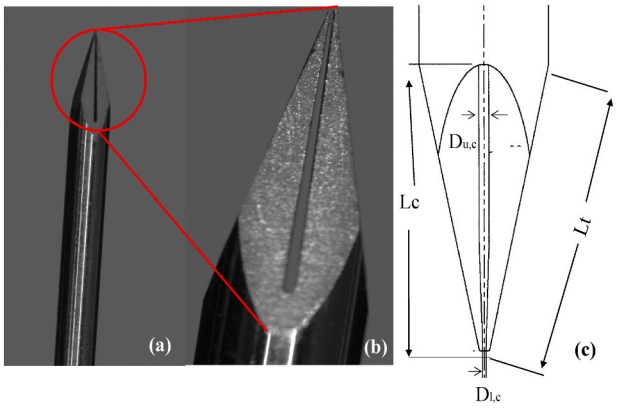

Fig. 1. (a,b) Optical microscope images of the printing pin at different magnifications; (c) sketch of the pin tip, where $D_{l,c} = 20$ μm, $D_{u,c} = 105$ μm, $L_c = 2$ mm, $L_t = 2.3$ mm.

0.01 pg/mL.

2.5. Aβ1–42 protein solution

We tested the technique for a biomarker of clinical interest, the Alzheimer's Aβ1–42 protein (Sigma Aldrich AG912). The white lyophilized powder was resuspended in 1% Ammonium hydroxide solution (NH_4OH) (Sigma-Aldrich 221,228) at concentration of 1 mg/mL according to manufacturing procedures, sonicated for 30 s and stored undiluted at −20 °C. Three dilutions were prepared with PBS 1× to obtain the final concentrations of 100 pg/mL, 20 pg/mL, 4 pg/mL.

2.6. Immunoreaction protocol

The Aβ1–42 was deposited by using the p-jet technique, afterwards the slide was incubated in a humid chamber for 2 h at 25 °C. For saturating excess protein-binding sites, the slide was covered with 2 mL of ArrayIt Blocking solution (BlockIt Blocking buffer) for 1 h at 25 °C. The blocking solution was used to dilute the antibody solutions. Then the slide was washed by placing it in a Petri dish with 10 mL of PBS 1× (Gibco 10010023) for 2 min. This washing cycle (WC) was repeated three times. A solution of primary antibody, 2 mL of rabbit anti-β-Amyloid 1–42 (Cell Signaling Technologies Rabbit D9A3A) at the dilution of 1:1600 was deposited on the slide and incubated overnight at 4 °C. The WCs were repeated. Finally, the secondary antibodies solution (Thermo Fisher Scientific anti-Rabbit I A32733), at the concentration of 0.5 μg/mL, was incubated 1 h at 25 °C and the WCs were repeated.

2.7. Microarray scanner

A confocal fluorescence microarray scanner InnoScan 710 (Innopsys) was used for measuring the fluorescence signal (FS) emitted by the spots obtained on the target slide by the p-jet accumulation. The imaging system used the laser source at 635 nm for exciting the fluorescent molecules and two digital photomultipliers (PMT) for recording the optical signal emitted by the molecules. Depending on the expected spot size and signal intensity, four main scan parameters can be adjusted: resolution (from 3 to 40 μm/pixel), speed (from 10 to 35 lines/s), gain PMT (linear from 0 to 100%), laser power (5 and 10 mW). The TIFF 16-bit images captured by the scanner were evaluated quantitatively by Mapix software.

2.8. The piezo-driven biospotter

The performance of the p-jet accumulation was compared to a commercial piezo driven biospotter (S3 sciFLEXARRAYER, Scienion AG) using a set of fluorophore samples. S3 is a non-contact dispensing system designed to produce small sample spots from ultra-low volumes of biomaterials. Samples were dispensed on top of low auto-fluorescence glass microscope slides (Marienfeld, ref. 1010200) after a washing procedure, where the slides were first rinsed with acetone and isopropanol, and then dried with nitrogen blow (Topgun). Fluorophore samples were prepared by diluting Alexa Fluor 647 carboxylic acid tris(triethylammonium) salt (A33084 Invitrogen) in 12 mM PBS (pH 7.4) to achieve fluorophore concentrations for three ranges: (1) 0.01 pg/mL to 10 pg/mL, (2) 10 ng/mL to 1 μg/mL and (3) 3 μg/mL to 12.5 μg/mL. The dispensed individual drop size with S3 was 350–372 pL and distance between the nozzle and the sample slide was 282–500 μm. Three replicate sample slides were prepared for the three concentration ranges. The schemes followed for dispensing drop samples were shown in the Supplementary Materials (S.1).

3. Results and discussion

3.1. Reproducibility of the p-jet spots

The p-jet sensor was used for accumulating the diluted biomolecules. In the last years, we have demonstrated for the first time the possibility of using the pyroelectric effect for accumulating micro-droplets and for detecting highly diluted biomolecules [22–24]. Here, we present a completely new configuration where we developed a more compact and easier-to-use heating system, compared to the CO_2 laser head or the μ-heater used in our first papers mentioned above. Due to figure limits, the complete description of this advanced experimental setup, as well as the thermal stimulus for generating the pyroelectric effect, are thoroughly described in the Supplementary material (S.2). Specifically, Fig. 2 in the Supplementary Material (S.2) shows the schematic of the experimental setup. Compared to our previous papers [22–24] here the bulky and high-power CO2 laser is replaced by an easy-to-use tungsten wire for the heating stimulation, thus opening the route toward a more compact setup. Moreover, the low power of the tungsten heating stimulation significantly reduces the occurrence of detrimental crystal breaks. In addition, the sample was loaded in those first papers by the Hamilton syringe as a sessile drop because the meniscus profile depended significantly on the volume of the drop, which had to fall in the submicrolitre range. Here the sample is loaded through a standard stealth pin and the higher load volume allows us to produce a higher number of droplets, with a significantly improved repeatability and better capability of concentration.

The reproducibility of the spots generated by this new configuration of p-jet sensor was evaluated by printing around 100 replicates of spots obtained by delivering 1 to 5 droplets and 10 to 50 droplets at each position. The successive droplets are indicated here as jets, for brevity. The sample was the Alexa fluorescent probe (see Materials and Methods) at 6 μg/mL concentration. Soon after the delivery of one spot, we translated the target slide by 1 mm by the precision translation stage, and we proceeded with the successive spots. Fig. 2(a) shows a typical scanner image of the resulting spots, just as an example.

The recorded scanner images were analyzed by Mapix software and the reproducibility of the technique in terms of diameter and FS is represented through the % coefficient of variation in Fig. 2(b). In particular, the diameter of the spots was on average 75 μm with a coefficient of variation of 5% for spots in the range 1–5 jets and 130 μm with a coefficient of variation of 7% for spots in the range 10–50 jets. Therefore, the variation of spot diameter was negligible with the increasing number of jets in both ranges. The FS data were analyzed

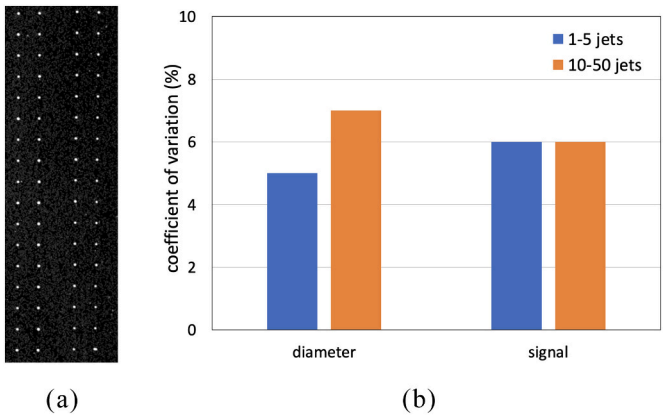

Fig. 2. (a) Scanner image of the typical p-jet spots obtained by spotting droplets of Alexa fluorescent probe; (b) coefficient of variation evaluated for the spot diameter and for the fluorescence signal in case of 1–5 jets (blue columns) and 10–50 jets (orange columns). (For interpretation of the references to colour in this figure legend, the reader is referred to the web version of this article.)

indifferently through 'F tot' or 'F mean' in the case of the p-jet spots. In fact, the first represents the sum of the gray values of all the pixels in the spot area and the second is F tot divided by the number of pixels in the spot area. In other words, the F mean values give information about the optical density of the spots. The FS had a variability of around 6% for the different groups of replicates at the same number of jets (see Fig. 2(b)). These results demonstrate the significance of the data and the high repeatability of the p-jet spots in terms of both diameter and intensity.

The commercial printing approaches are usually classified as contact and non-contact printing. Contact printing typically uses a pin, which is usually designed from stainless steel, titanium, or tungsten. Contact printing has several drawbacks such as the deformation of the tip, which introduces imprecision about deposition [26–28], or the contaminations of the biological samples. Conversely, the non-contact printing heads, such as those based on piezoelectric nozzles, eject the sample droplets from a specific distance [29], thus avoiding contact-related issues. However, failed spots, satellite spots, and misplaced spots [30] may occur in this modality. Here, the outstanding novelty of the pin-based p-jet is that the ejection of tiny droplets from the capillary of the stealth pin is achieved through an electrostatic interaction at short distances, thus preserving the spatial precision of contact printing, but at the same time avoiding the typically related drawbacks.

3.2. Characteristic curves of the p-jet accumulation

To test the reliability of this new p-jet sensor for tuning the accumulation rate of low abundant biomolecules, we evaluated the behavior of the FS of the spots as a function of the number of droplets (referred to as jets) delivered for each spot. It is well known that ELISA-based procedures represent the gold standard in most clinical diagnoses aimed to detect specific biomarkers in human fluids. Detection of Aβ1–42 in human cerebrospinal fluid for Alzheimer's disease diagnosis is challenging for ELISA having a nominal limit of detection (LOD) of 50 pg/mL, which prevents a reliable detection of these biomarkers in peripheral fluids such as blood, where the concentrations are expected to reach only sub-picogram levels. Considering the novelty of the technique, we performed this study first for three relatively high concentration values in the μg/mL range (12; 6; 3) and successively for three challenging concentrations (10 pg/mL; 0.1 pg/mL; 0.01 pg/mL).

We loaded the pin with the Alexa probe sample at 12.5 μg/mL and we printed five spots, the first with one jet and the others by accumulating two jets, three jets, four jets and five jets, respectively. We performed eight replicates for each spot, and we repeated the same kind of experiment for the other two concentrations at 6 μg/mL and 3 μg/mL. Fig. 3 shows the behavior of the FS as a function of the number of accumulated jets for the three concentrations at the μg/mL level.

The dashed lines correspond to the background level calculated as three times the standard deviation of the background signal. The data on the Y axis correspond to the average FS over eight replicates of the spots calculated as mean gray values per unit area of the spots. These results show that the optical density of the spots increased linearly with increasing number of accumulated jets for each concentration, and the linear regression equations exhibited $R^2 \geq 0.98$.

After appropriate cleaning of the printing pin, we loaded the labelled antibody probe solution (see Materials and Methods) at the concentration of 10 pg/mL and we printed ten spots with an increasing number of jets from one to ten. On the same target slide, we deposited ten spots obtained by simply touching the slide with the printing pin from one to ten times for each spot. We performed three replicates of the spots and we recorded the fluorescence images of the slides by the scanner. The images were analyzed by Mapix and the resulting data were averaged over three replicates. Fig. 4(a) shows the corresponding graph.

The results in Fig. 4(a) demonstrate clearly that the contact-based accumulation does not behave linearly over the range of 1–10 touches, due to the cross contamination occurring in successive touches of the pin on the same spot location. Moreover, the contact nature of this print method also means that during every deposition there is a chance that the pin tip may be damaged, thus worsening the repeatability in the deposited volume at each touch [31,32]. The lack of reliability is evident also through the behavior of the FS in the spots obtained with a few touches, where the signal is not detectable significantly over the background level. Conversely, the FS of the spots obtained by p-jet accumulation at 10 pg/mL is significantly higher than the background level, even for few jets with an average signal/noise ratio (SNR) of 90 at one and two jets. Analogously to the case with Alexa probe, also in this case the data show that the optical density of the spots increased linearly with the increasing number of accumulated jets, with linear regression equations exhibiting $R^2 \geq 0.99$.

We performed the same kind of characterization for two concentrations at 0.1 pg/mL and 0.01 pg/mL to test the reliability of the p-jet accumulation at very challenging levels of concentration. Considering the two and three orders of magnitude decrease in concentration we tested the accumulation effect by using a higher number of jets, from 10 to 50 at a step of 10. We performed three replicates of the spots also in this case and we recorded the fluorescence images of the slides by the scanner. The images were analyzed by Mapix and the resulting data were averaged over the three replicates (see Fig. 4**(b,c)**). In both samples, the SNR ranged from 6 to 14 and the spot optical density increased linearly in the whole range of jets. These results demonstrate the reliability of the p-jet in tuning linearly the rate of accumulation of biomolecules by the number of jets and in detecting fluorescence-labelled Ab2 proteins at challenging concentrations, thanks to the significant increase of the optical density.

3.3. Comparative study with S3 biospotter dispensed samples

We performed a comparative study with a commercial piezo-driven S3 biospotter, which is an established printing method, by using the same samples. S3 was used to dispense eight replicate sample spots with one to five dispensed jets at each position. The sample was the Alexa

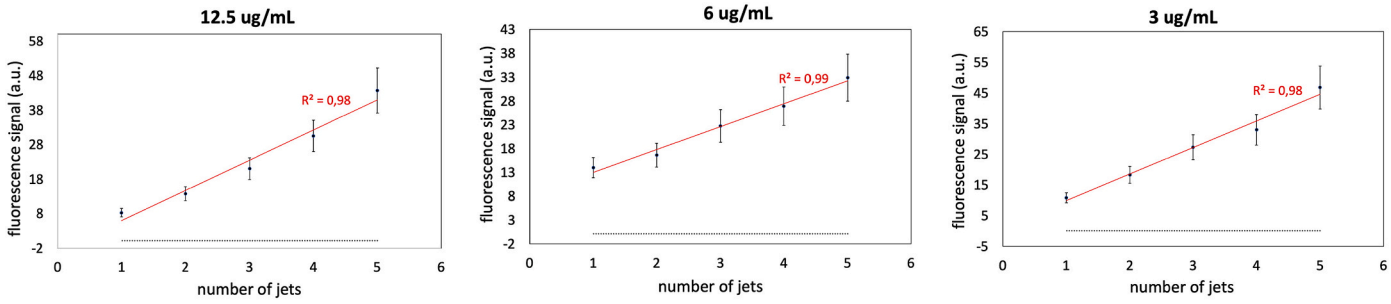

Fig. 3. Fluorescence signal of the p-jet spots as a function of the increasing number of jets, for three concentrations of the Alexa probe. The signal values were averaged over eight replicates of the spots and the error bars correspond to their standard deviation. The linear plots were obtained by least squares fitting. The horizontal dashed lines correspond to the background level calculated as three times the standard deviation of the background FS.

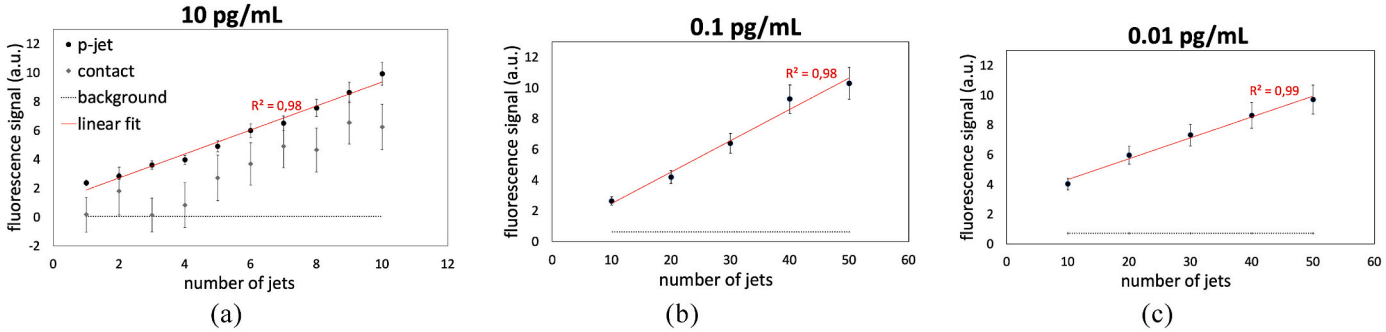

Fig. 4. Fluorescence signal of the p-jet spots for an increasing number of jets of the labelled antibody sample in case of (a) 10 pg/mL; (b) 0.1 pg/mL; (c) 0.01 pg/mL. In (a) we also report the results in the case of 10 pg/mL by contact printing. The data in (a-c) were averaged over three replicates of the spots with error bars corresponding to their standard deviation. The linear plots were obtained by least-squares fitting. The horizontal dashed lines correspond to the background level calculated as three times the standard deviation of the background signal.

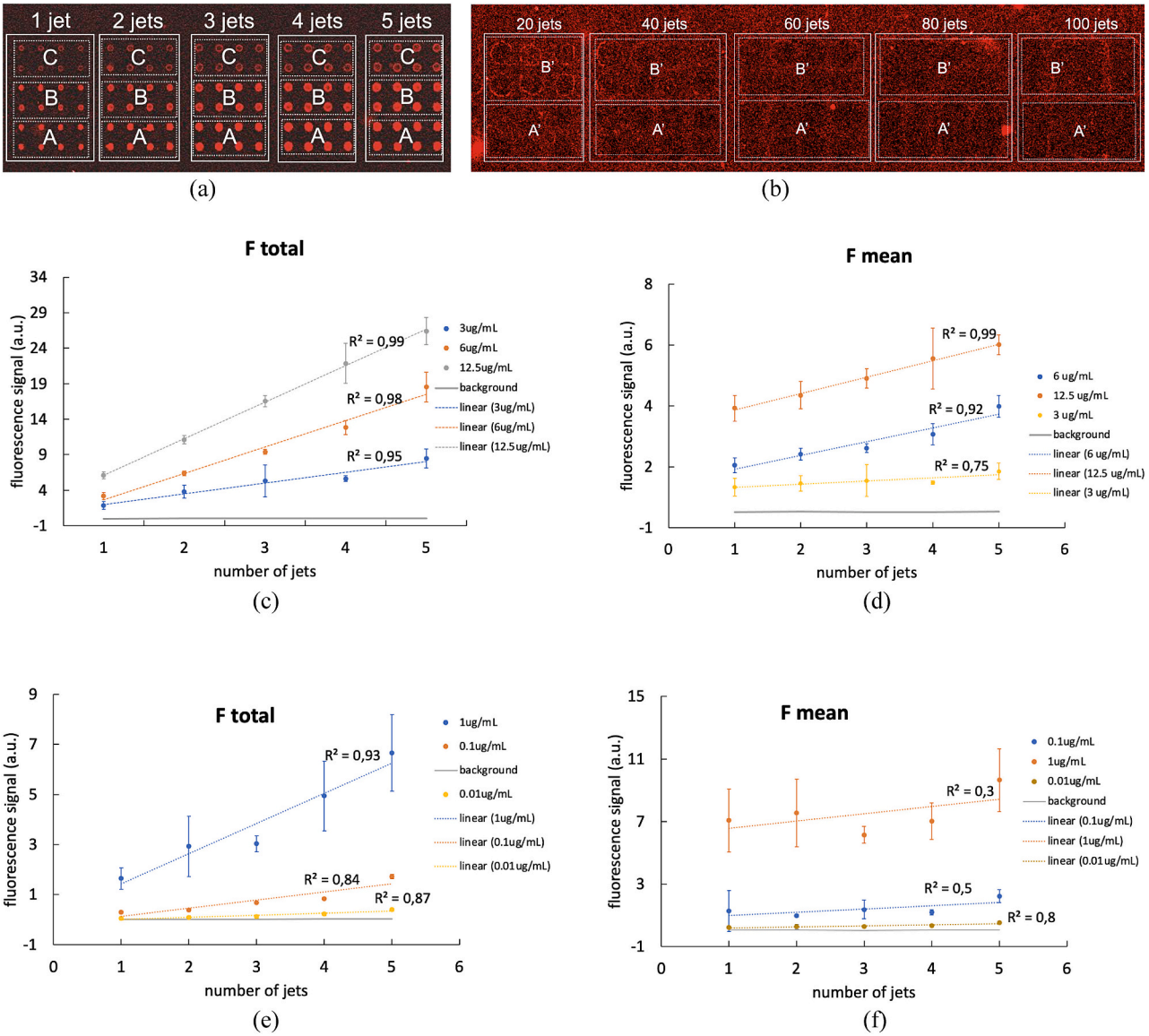

Fig. 5. Biospotter results. (a,b) Typical scanner images of the slides with the spots at 1 μg/mL (A), 0.1 μg/mL (B), 0.01 μg/mL (C), 0.1 pg/mL (A') and 0.01 pg/mL (B′); (c,e) F tot as a function of the number of jets for the concentrations in the ranges 12.5 μg/mL-3 μg/mL and 1 μg/mL-0.01 μg/mL, respectively; (d,f) F mean as a function of the number of jets for the concentrations in the ranges 12.5 μg/mL-3 μg/mL and 1 μg/mL-0.01 μg/mL, respectively. The data in (c-f) were averaged over eight replicates of the spots with error bars corresponding to their standard deviation. The linear functions were obtained by the weighted least-square method. The average diameter in (a) is 300 μm for 1 jet and 600 μm for 5 jets.

fluorescent probe (see Materials and Methods). The behavior was evaluated as a function of the number of jets for different concentration ranges. The first concentration range included 12.5 μg/mL – 6 μg/mL – 3 μg/mL, the second 1 μg/mL - 0.1 μg/mL - 0.01 μg/mL, the third 10 pg/mL - 0.1 pg/mL - 0.01 pg/mL. The FS was measured by the scanner, and the images were analyzed by the Mapix software. Fig. 5**(a,b)** shows the typical scanner images of the slides with spots at the second and third concentration ranges, respectively. Fig. 5(a) shows that the spot diameter increased significantly with the number of jets, on average from 300 μm (1 jet) to 600 μm (5 jets), and Fig. 5(b) shows the lack of significance of the spots at the challenging dilutions. The FS was analyzed here in terms of both F tot and F mean values and Fig. 5**(c-f)** show the corresponding results.

Both F tot and F mean increase with the number of jets for all the concentration ranges. However, while F tot increases on average by a factor of five and six in the first and second concentration range respectively (see Fig. 5**(c,e)**), the F mean increases only by a factor of two in all samples (see Fig. 5**(d,f)).** This means that the increase in spot optical density is negligible for increasing jets, thus preventing the accumulation effect achieved instead by p-jet. In fact, the spots at challenging concentrations have SNR < 1, even up to 100 jets (see Fig. 5 (b)**).** Moreover, linear regressions with $R^2 \geq 0.98$ were achieved only for the F tot values at 12.5 μg/mL and 6 μg/mL and for F mean values at 12.5 μg/mL, thus demonstrating the lack of linear behavior for all the concentrations below the μg/mL level.

The results of this comparative study demonstrate the ability of the p-jet to accumulate efficiently biomolecules and to make them detectable through the higher density of the FS, even down to sub-picogram concentrations of the mother sample. The results achieved in case of the biospotter show how such detection capability is not reachable through a commercially available micro-droplet spotter. Therefore, we believe that this p-jet technique would open the route to the development of a highly sensitive device for early diagnosis applications.

3.4. *Application for immunodetection of Aβ1–42*

The p-jet sensor was tested in case of a typical application where the target molecules are detected through an immunofluorescence reaction. The target molecule was the protein Aβ1–42, which belongs to the family of biomarkers object of clinicians' interest in the diagnosis of AD. We tested the p-jet technique on a set of three solutions (500 pg/mL; 50 ng/mL and 50 μg/mL) covering a relatively large range of concentrations, to test the applicability of the immunoreaction protocol on spots of proteins made of 20 accumulated p-jets. Three spots were produced for each concentration value. The spot images were recorded by the scanner and evaluated by Mapix and Fig. 6 shows the resulting data averaged over the replicates of the spots.

The FS increases clearly with increasing concentration of the protein, and the signal-to-noise ratio was around 16 on average in all the spots. These results demonstrate the reliability of the p-jet spots for detecting target molecules in a more real case study, namely not labelled proteins, such as the Aβ1–42 protein used in this test. The molecules are accumulated successfully onto a solid reaction slide and detected through an a-posteriori immunoreaction protocol. In perspective, this technique would simplify the detection of low abundant biomolecules by accumulating them directly onto the reaction slide and by using sub-microliter volumes of reaction, with significant advantages in all those cases where diagnostic applications must be performed with very small volumes of analyte.

4. Conclusions

We have presented a new p-jet sensor with the ability to enhance the fluorescence signal of low abundant biomolecules linearly by increasing the number of accumulated jets. This technique provides an easy-to-use procedure that can tune the accumulation rate of target molecules in highly diluted solutions. The reliability of the proposed system has been demonstrated by the linear behavior of the fluorescence signal as a function of the probe concentration. We performed a comparative study with the same reagents using a commercial piezo-driven biospotter which is an established printing method. The results of this comparative study demonstrate the ability of the p-jet sensor to push the detection limit down to the sub-picogram level against the microgram level achieved in the case of the biospotter. Moreover, the technique has been demonstrated to be compatible with a typical immunofluorescence detection method applied to the protein Aβ1–42, a well-known biomarker of AD. In perspective, this p-jet technique can be exploited in a wide range of clinical cases where the clinician needs to detect low abundant biomarkers in peripheral body fluids, especially when only small volumes of samples are available.

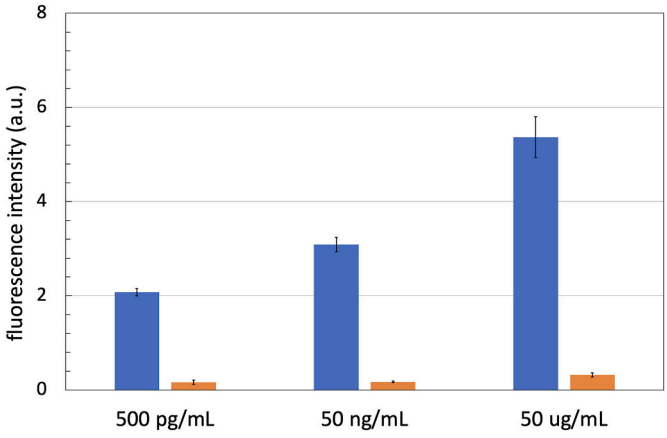

Fig. 6. Mean fluorescence intensity of the p-jet spots of Aβ1–42 (blue columns) and of the background (orange columns) at different solution concentrations. The error bars represent the standard deviation over the replicates. (For interpretation of the references to colour in this figure legend, the reader is referred to the web version of this article.)

Declaration of Competing Interest

The authors declare that they have no known competing financial interests or personal relationships that could have appeared to influence the work reported in this paper.

Acknowledgments

The authors acknowledge the EU funding within the Horizon 2020 Program, under the FET-OPEN Project “SensApp”, Grant Agreement n.829104. In addition to “SensApp”, VTT researchers acknowledge the support of the Academy of Finland Flagship Programme, Photonics Research and Innovation (PREIN), decision 320168. The CNR authors acknowledge Romina Rega for her collaboration in preparing the glass slides. The CNR authors acknowledge the Innovation & Technology Provider S.r.l. and Heinz Italia S.p.A. for funding under the project code B51I18000840007. The VUB research was supported by the Methusalem program of the Flemish government and Hercules foundations and the Scientific Research Council (OZR) of the Vrije Universiteit Brussel (VUB). Y. Nie acknowledges Research Foundation Flanders (FWO) for her post-doctoral fellowship (No. 1252722N).

Appendix A. Supplementary data

Supplementary data to this article can be found online at https://doi.org/10.1016/j.sbsr.2022.100536.

References

[1] P. Mehrotra, Biosensors and their applications - a review, J. Oral Biol. Craniofacial. Res. 6 (2) (2016) 153–159, https://doi.org/10.1016/j.jobcr.2015.12.002.

[2] M. Ngoepe, et al., Integration of biosensors and drug delivery technologies for early detection and chronic management of illness, Sensors (Switzerland) 13 (6) (2013) 7680–7713, https://doi.org/10.3390/s130607680.

[3] J. Brooks, B. Mirhabibollahi, R. Kroll, J. Brooks, B. Mirhabibollahi, R. Kroll Experimental enzyme linked amperometric immunosensors for the detection of Salmonella in foods, J. Appl. Bact. 73 (1992) 189–196.

[4] S.M. Radke, E.C. Alocilja, A high density microelectrode array biosensor for detection of *E. coli* O157:H7, Biosens. Bioelectron. 20 (8) (2005) 1662–1667, https://doi.org/10.1016/j.bios.2004.07.021. SPEC. ISS.

[5] J. Wang, Electrochemical glucose biosensors, Chem. Rev. 108 (2) (2008) 814–825, https://doi.org/10.1021/cr068123a.

[6] C. Li, Y. Yang, D. Wu, T. Li, Y. Yin, G. Li, Improvement of enzyme-linked immunosorbent assay for the multicolor detection of biomarkers, Chem. Sci. 7 (5) (2016) 3011–3016, https://doi.org/10.1039/c5sc04256a.

[7] Y. Chen, J. Liu, Z. Yang, J.S. Wilkinson, X. Zhou, Optical biosensors based on refractometric sensing schemes: a review, Biosens. Bioelectron. 144 (August) (2019) 111693, https://doi.org/10.1016/j.bios.2019.111693.

[8] B. Gil Rosa, et al., Multiplexed immunosensors for point-of-care diagnostic applications, Biosens. Bioelectron. 203 (October 2021) (2022) 114050, https://doi.org/10.1016/j.bios.2022.114050.

[9] W. Wang, C. Chen, M. Qian, X.S. Zhao, Aptamer biosensor for protein detection using gold nanoparticles, Anal. Biochem. 373 (2) (2008) 213–219, https://doi.org/10.1016/j.ab.2007.11.013.

[10] S. Galozzi, K. Marcus, K. Barkovits, Amyloid-β as a biomarker for Alzheimer's disease: quantification methods in body fluids, Expert Rev. Proteom. 12 (4) (2015) 343–354, https://doi.org/10.1586/14789450.2015.1065183.

[11] M. Vestergaard, K. Kerman, E. Tamiya, An overview of label-free electrochemical protein sensors, Sensors 7 (12) (2007) 3442–3458, https://doi.org/10.3390/s7123442.

[12] A. Piriya, V.S, P, K. Daniel S.C.G. Joseph, S. Lakshmanan, T. Kinoshita, S. Muthusamy, Colorimetric sensors for rapid detection of various analytes, Mater. Sci. Eng. C 78 (2017) 1231–1245, https://doi.org/10.1016/j.msec.2017.05.018.

[13] Y. Kitamura, et al., Plasma protein profiling for potential biomarkers in the early diagnosis of Alzheimer's disease, Neurol. Res. 39 (3) (2017) 231–238, https://doi.org/10.1080/01616412.2017.1281195.

[14] C. Humpel, Identifying and validating biomarkers for Alzheimer's disease, Trends Biotechnol. 29 (1) (2011) 26–32, https://doi.org/10.1016/j.tibtech.2010.09.007.

[15] A. Nakamura, et al., High performance plasma amyloid-β biomarkers for Alzheimer's disease, Nature 554 (7691) (2018) 249–254, https://doi.org/10.1038/nature25456.

[16] S. Janelidze, et al., Plasma β-amyloid in Alzheimer's disease and vascular disease, Sci. Rep. 6 (March) (2016) 1–11, https://doi.org/10.1038/srep26801.

[17] P.E. Khoonsari, et al., Improved differential diagnosis of Alzheimer's disease by integrating elisa and mass spectrometry-based cerebrospinal fluid biomarkers, J. Alzheimers Dis. 67 (2) (2019) 639–651, https://doi.org/10.3233/JAD-180855.

[18] O. Gennari, et al., A skin-over-liquid platform with compliant microbumps actuated by pyro-EHD pressure, NPG Asia Mater. 11 (1) (2019) 1–8, https://doi.org/10.1038/s41427-018-0100-z.

[19] R. Rega, O. Gennari, L. Mecozzi, S. Grilli, V. Pagliarulo, P. Ferraro, Bipolar patterning of polymer membranes by pyroelectrification, Adv. Mater. 28 (3) (2016) 454–459, https://doi.org/10.1002/adma.201503711.

[20] L. Mecozzi, O. Gennari, R. Rega, L. Battista, P. Ferraro, S. Grilli, Simple and rapid bioink jet printing for multiscale cell Adhesion Islands, Macromol. Biosci. 17 (3) (2017) 1–6, https://doi.org/10.1002/mabi.201600307.

[21] R. Rega, O. Gennari, L. Mecozzia, S. Grilli, V. Pagliarulo, P. Ferraro, Pyro-electrification of polymer membranes for cell patterning, AIP Conf. Proc. 1736 (May) (2016) 2016, https://doi.org/10.1063/1.4949617.

[22] S. G. R. Rega, J. F. Muñoz Martinez, M. Mugnano, E. Oleandro, O. Gennari, P. Orlando, G. Cabassi, V Pelizzola, P. Ferraro, "A pyroelectric-based system for sensing low abundant lactose molecules," Proc. Opt. Methods Insp. Charact. Imag. Biomater. IV, vol. 110.

[23] R. Rega, et al., Detecting collagen molecules at picogram level through electric field-induced accumulation, Sensors (Switzerland) 20 (12) (2020) 1–11, https://doi.org/10.3390/s20123567.

[24] S. Grilli, et al., Active accumulation of very diluted biomolecules by nano-dispensing for easy detection below the femtomolar range, Nat. Commun. 5 (2014) 1–6, https://doi.org/10.1038/ncomms6314.

[25] M. Schena, D. Shalon, R.W. Davis, P.O. Brown, Quantitative monitoring of gene expression patterns with a complementary DNA microarray, Science (80-.). 270 (5235) (1995) 467–470, https://doi.org/10.1126/science.270.5235.467.

[26] R. Safavieh, M. Pla Roca, M.A. Qasaimeh, M. Mirzaei, D. Juncker, Straight SU-8 pins, J. Micromech. Microeng. 20 (5) (2010), https://doi.org/10.1088/0960-1317/20/5/055001.

[27] V. Romanov, S.N. Davidoff, A.R. Miles, D.W. Grainger, B.K. Gale, B.D. Brooks, A critical comparison of protein microarray fabrication technologies, Analyst 139 (6) (2014) 1303–1326, https://doi.org/10.1039/c3an01577g.

[28] B.J. Helka, J.D. Brennan, A guided materials screening approach for developing quantitative sol-gel derived protein microarrays, J. Vis. Exp. 78 (2013) 1–13, https://doi.org/10.3791/50689.

[29] P.M. Theiler, F. Lütolf, R. Ferrini, Non-contact printing of optical waveguides using capillary bridges, Opt. Express 26 (9) (2018) 11934, https://doi.org/10.1364/oe.26.011934.

[30] I. McWilliam, M.C. Kwan, D. Hall, Inkjet printing for the production of protein microarrays, Methods Mol. Biol. 785 (2011) 345–361, https://doi.org/10.1007/978-1-61779-286-1_23.

[31] P. Gong, D.W. Grainger, Comparison of DNA immobilization efficiency on new and regenerated commercial amine-reactive polymer microarray surfaces, Surf. Sci. 570 (1–2) (2004) 67–77, https://doi.org/10.1016/j.susc.2004.06.181.

[32] R.A. George, J.P. Woolley, P.T. Spellman, Ceramic capillaries for use in microarray fabrication, Genome Res. 11 (10) (2001) 1780–1783, https://doi.org/10.1101/gr.190801.